Selected observations from avalanche measurements at the Ryggfonn test site and comparisons with observations from other locations

Peter Gauer*

Norwegian Geotechnical Institute

Sognsveien 72, NO-0855 Oslo, Norway

ABSTRACT. Selected observations from the full-scale avalanche test site Ryggfonn, Norway, like front velocity, runout distance, or pressure distributions, are presented and compared with observations from other locations. In this way, data are provided that could be used as reference in the process of hazard zone delimitation or while evaluating the performance of computational runout models.

Keywords: avalanche observations, comparison, hazard mapping

1 INTRODUCTION

Snow avalanches pose a deadly peril to human and a danger to their belongings ever since human started to settle in mountainous regions. Numerous historical accounts tell stories about catastrophic events that wiped out whole families or even villages. Figure 1, for example, shows data on building damages in Norway during the period from 1600 to 2015. For this period a total number 902 of records about damages due to snow avalanches (disregarding slushflows) exist. In addition, a significant number of unreported cases, even in recent years, can be expected. Furthermore, the total number of destroyed or damaged buildings is uncertain as some records subsume a series of destructions. A frequency analysis implies a return period of around 10 years for major event cycles (i.e. years with 5 and more records). According to these data, the most destructive winter was the winter 1867/1868 with 52 records.

The remnants of historic avalanche defense structures and old rules, like the declarations of avalanche forests, bear witness to long-term efforts of inhabitants to protect themselves and their property against avalanches. Those early protection measures were mostly based on trial and error approaches. In the Alps, a more scientific or engineering approach started in the second half of the 19th century with persons like J. Coaz, and later with W. Paulcke and with institutions such as Swiss Avalanche Commission and

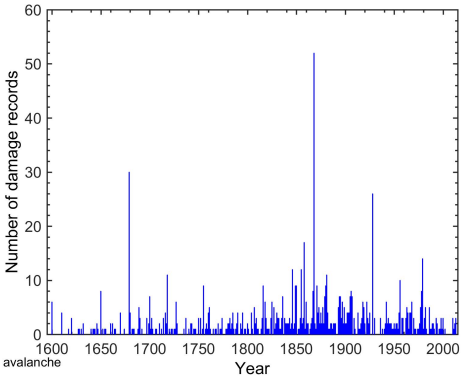

Figure 1: Records of building damages in Norway during the period from 1600 to 2015 (data based on NVEs net-site “http://www.skrednett.no/”).

in Austria with the establishment of the Austrian Service for Torrent and Avalanche Control. With this more scientific approach to avalanche protection the need to a better understanding of the avalanche flow itself was needed and systematic measurements started.

In the aftermath of the avalanche catastrophes in the Alps in 1952 and 1954, a large focus was put on the establishment of permanent defense structures. A series of avalanche catastrophes in the second half of the 20th century turned the focus on the identification of avalanche hazard zones and their integration in landuse planning, which is today standard in risk management in many countries. In the process to delimit the endangered avalanche zones, the use of computer models like RAMMS (Christen et al., 2010); SAMOS-AT (Sampl and Granig, 2009) or N2L (Naaim et al., 2004) become more and more customary. Although, those models are still far from perfect. For example,

*Corresponding author's address:
Peter Gauer
Norwegian Geotechnical Institute,
P.O. Box 3930 Ullevål Stadion, NO–0806 Oslo, Norway
Tel: ++47 45 27 47 43; Fax: ++47 22 23 04 48; E-mail: pg@ngi.no

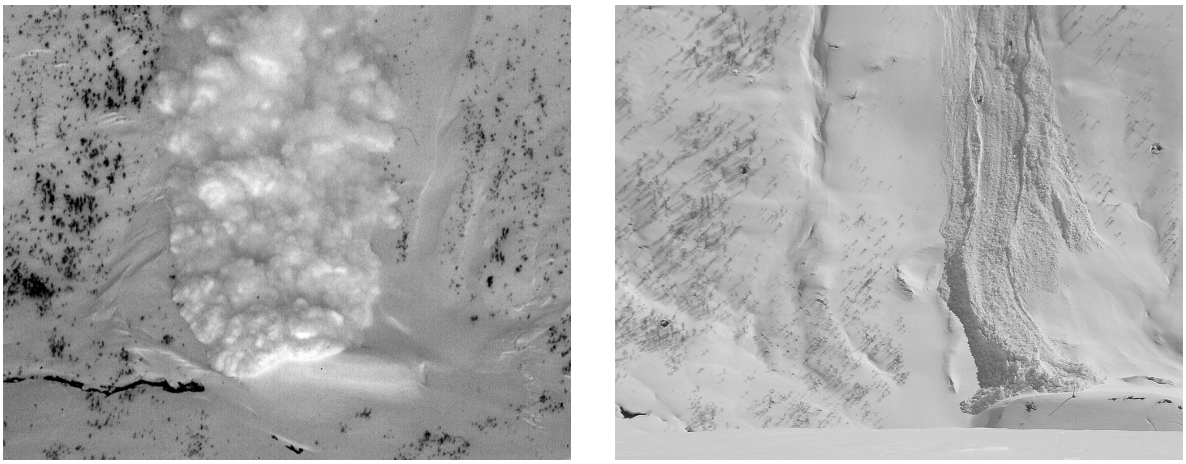

Figure 2: Dry-mixed avalanche 2000-02-17 (left) surpassing the catching dam in the "runout area" of the Ryggfonn test site and avalanche 2005-04-16 (right), which started as dry snow avalanche but run into damp snow in the valley bottom. Both avalanches are still in motion at the time of the photograph. (photos K. Kristensen and A. Moe, NGI)

a major challenge for those models is to capture the transition between flow regimes during an avalanche descent (see Fig. 2). Some of present models also show a tendency to underestimate the maximum velocity along the track while reproducing the runout distance reasonably.

Snow avalanches, likewise debris flows, rockslides and rock avalanches, or submarine slides can be classified as gravity mass flows. That is, the driving force for their motion is gravity and motion is caused by a density difference between the slide and the ambient medium—in the case of snow avalanches this is air. A change in flowing density as expected during a flow regime alternation will have a major effect on the dynamics of the flow—vice versa— (Gauer et al., 2008a). Although avalanches have been classified as dense (/wet) or powder snow avalanches (UNESCO, 1981) for a long time, still little is known how exactly ambient conditions, like snowpack properties and air temperature, influence the avalanche dynamics. To gain a better understanding of these interdependencies, avalanche experiments are still necessary—also full scale tests. In the end, these interdependencies are decisive for the avalanche runout distance (Fig. 2), impact, and their return period; and therefore important for risk management.

However, as long as the physics behind avalanche flows is not fully understood, it is important for practitioners to have some idea about the order of expected magnitudes of relevant avalanche parameters. In the following a collection of some of those data are presented.

2 FULL-SCALE AVALANCHE TEST SITES

As mentioned above, with the scientific approach to avalanche protection and hazard mapping the need to a better understanding of the avalanche flow arose. Dedicated test sites were established at various locations around the world, like in the Khibins, Kola Peninsula, Russia; Roger Pass, Canada; or Kurobe Canyon, Japan (for references see Gauer et al., 2010a). An overview of European avalanche test sites can be found in Barbolini and Issler (2006) or in more recent descriptions of specific test sites (Ammann, 1999; Gauer et al., 2010a; Maggioni et al., 2012), and (Thibert et al., 2015). Those test sites have been equipped with various kinds of sensors to measure, for example,

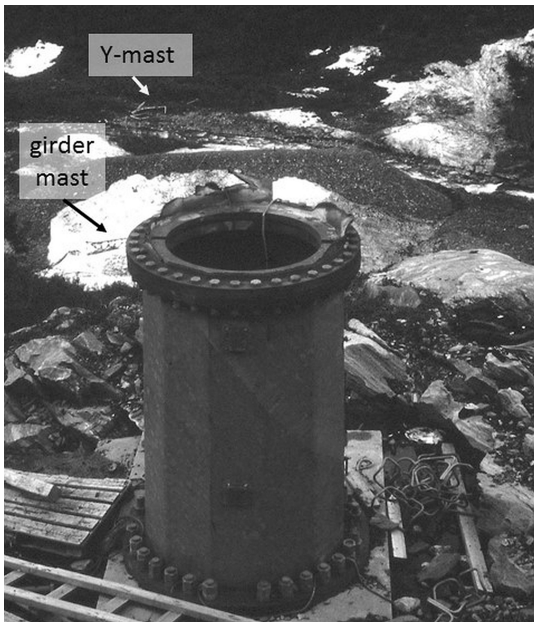

Figure 3: Remains of the Y-mast after the destructive avalanche event 1990-04-01 at Ryggfonn (photo NGI). The top part of the mast was bent off and swept downside of the catching dam by the avalanche. In front of the catching dam are the remains of a girder mast that belonged to a power line assembly.

impact pressure or avalanche velocities. The assortment of sensors including pressure cells, geophones, video, optical velocity sensors or Doppler radar, just to name some, gave valuable insights into avalanche dynamics. The harsh conditions within an avalanche, however, make full-scale tests difficult and costly and most of the test sites experienced at least once a destructive event (see Figure 3).

3 SELECTED OBSERVATIONS FROM AVALANCHE MEASUREMENTS

As some of the measurements might be site-specific, it is important to compare these measurements to uncover scaling effects. In the following, a series of selected observations from measurements at the Ryggfonn test site are presented and in part compared with observations from other locations (not necessary only to data from test sites). These data give an indication of the expected order of magnitude depending on, e.g., the path geometry.

3.1 Mean retarding acceleration

A well-known empirical relation is the so-called α-β model by Lied and Bakkehøi (1980), which relates the runout angle, α (i.e. the so-called "Fahrböschungswinkel"), to the average inclination of the path, β, based on several hundred avalanche observations of "extreme events" (i.e. events with return periods of the order 100 years or more). Against to what one may expect, in its simplest form the model bases only on one geometrical property of the avalanche path—the β-angle. It does not bear any information on the absolute avalanche size. Figure 4 depicts several proposed model relationships for various mountain regions. Really obvious is a only deviation of the Colorado and Nevada data from the others. Also avalanches on short slopes (less than about 400 m) tend to have relatively longer runouts (i.e. lower α-angles). In addition, the figure shows α data from the Ryggfonn test site that correspond to different return periods between 1 and 40 years.

Gauer et al. (2010b) used α-β data to investigate the mean retarding acceleration,

$$|\langle a_{ret}\rangle| = g\frac{H}{S} \tag{1}$$

of these avalanches, where g is the acceleration due to gravity, H the fall height, and S is the total travel distance. The mean retarding acceleration is a measure of the energy dissipation per unit mass along the track, which does not use any assumptions about the underlying rheology. They found that the mean retarding acceleration could be approximated by

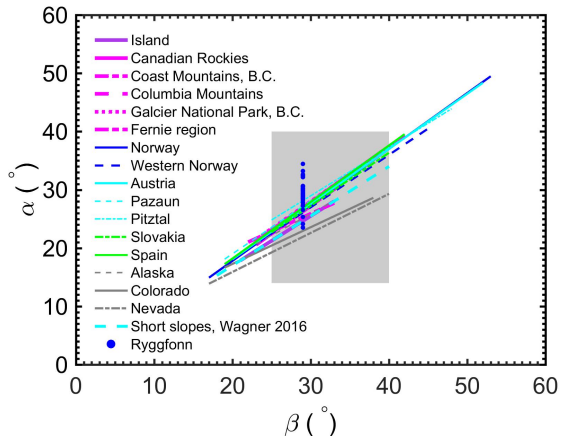

Figure 4: Comparison of proposed α-β relations for several mountain ranges (data adapted from McClung and Mears, 1991; Wagner, 2016, and references therein). The gray shaded area indicates the most relevant range. In addition, α values from avalanches at the Ryggfonn test site are shown.

$$\frac{\langle a_{ret}\rangle}{g} \approx \frac{a_{fit}}{g} = 0.82\sin\beta + 0.052 \tag{2}$$

This implies that the dissipation rate increases with increasing steepness of the path. Figure 5 shows this relation and data from selected observations for which information on the volume of deposition are available. It should be mentioned that these observations for

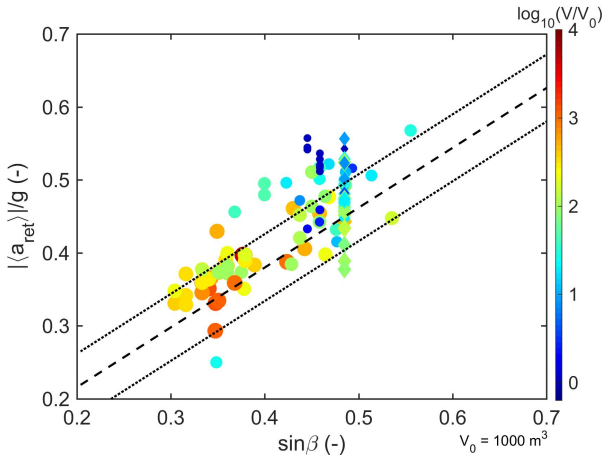

Figure 5: Mean retarding acceleration, $\langle a_{ret}\rangle$/g, vs. $\sin\beta$ based on several hundred avalanche observations. The dashed lines indicate the linear trend and the dotted lines mark the $\pm\sigma$ range. The points show avalanche events for which data on the volume of the deposit are available. Color and size of the marker indicate the magnitude of the deposit volume, $\log_{10}(V_{Dep}/V_0)$. Diamonds mark data from the Ryggfonn test site and circles show data originating from various locations (cf. Gauer et al., 2010b).

which the volume are available have the tendency to lay above the trend line based on all data. That is, these events had a shorter runout distance than one could expect, however, one should keep in mind not all of these events were necessarily the most extreme event relative to the respective path.

How the runout distance depends on the avalanche volume is shown in Figure 6. Here the observed retarding accelerations are de-trended by

$$\Delta_\beta \langle a_{ret} \rangle = a_{fit} - \langle a_{ret} \rangle \quad (3)$$

and plotted against the magnitude of the deposit volume, $\log_{10}(V_{Dep}/V_0)$, where V_0 is set to 1000 m^2. The sign is defined in that way that a positive value implies higher retardation and consequently shorter runout distances. The upper curve shows data from Ryggfonn and the lower one data from other locations. In the case of Ryggfonn, the gradient is about -0.032 and in the case of the lumped avalanche data, the gradient is -0.027. This suggests, larger avalanches tend to have on average longer runout distances. For typical values of $\langle a_{ret} \rangle / g$ between 0.3 and 0.6 an increase of the avalanche volume by a factor 10 may cause an elongation of the runout distance by about 5 to 10%. However, the p-value for the lumped data signifies little significance. If one excludes small events from the data set with volume less than 2000 m^3, which have a high Cook distance (i.e. these values have a high level of influence on the regression) the gradient decreases to -0.011. This suggests that the absolute value of the avalanche has little influence on the retardation of an avalanche, which is in accordance with

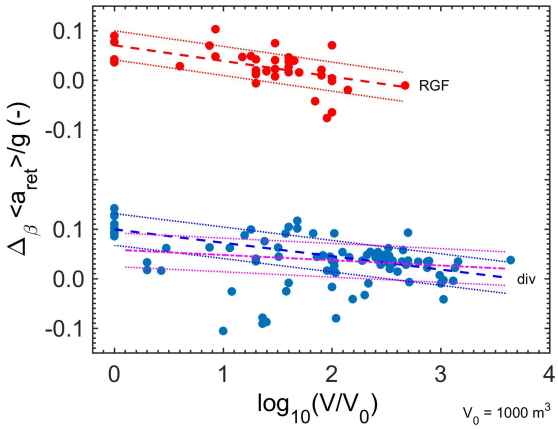

Figure 6: De-trended mean retarding acceleration, $\langle a_{ret} \rangle / g$, vs. the order of magnitude of the deposit volume, $\log_{10}(V_{Dep}/V_0)$. The dashed lines indicate the linear trend and the dotted lines mark the $\pm\sigma$ range. Magenta lines show a fit for avalanches disregarding small events with a volume less than 2000 m^3.

the empirical α-β model that does not bear information on size. Probably more significant is the relative size to the path at this point.

As a side remark, observations from Ryggfonn indicate that a 10 degree decrease in (air) temperature has a similar prolongation effect as a size increase of one order of magnitude (Gauer and Kristensen, 2016). For a discussion on temperature effects, the reader is also referred to Steinkogler et al. (2014).

3.2 Entrainment depth

The preceding paragraph gives some impression on how the avalanche volume may influence the runout distance. By now it is known that entrainment along the track contributes to a large degree to the mass balance of an avalanche (Sovilla et al., 2006; Gauer and Issler, 2004). Figure 7 presents estimations on the averaged erosion depth for Ryggfonn and for comparison, estimates from other locations. At Ryggfonn, avalanches entrained on average 0.25 m snow along the track. In comparison, the mean entrainment depth for the other observations is about 0.4 m. This higher value might be expected as these avalanches are regarded more extreme events on average. The esti-

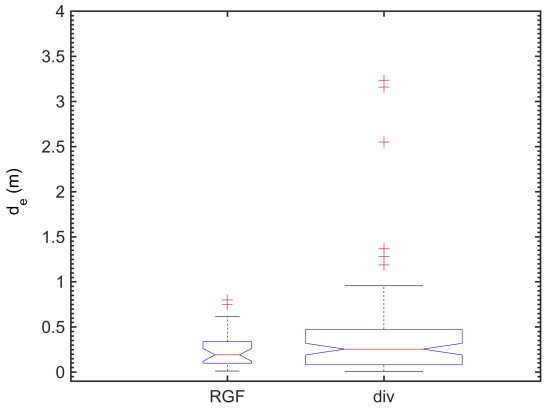

Figure 7: Averaged slope normal erosion depth, d_e. RGF mark observations made at the Ryggfonn test site and div refer to a compilation of observations from various avalanches path in the Alps and Norway (cf. Gauer et al., 2010b). The median is shown by the red central mark, the 25th–75th percentile as edges of the blue box, the whiskers extend to the most extreme data points not considered outliers and outliers are marked with a red cross (points larger than $q_3 + 1.5\,(q_3 - q_1)$ or smaller than $q_1 - 1.5\,(q_3 - q_1)$, where q_1 and q_3 are the 25th and 75th percentiles). The notched area signifies a 95% confidence interval for the median. The width of the box indicates the relative number of measurements (noe = 28/90).

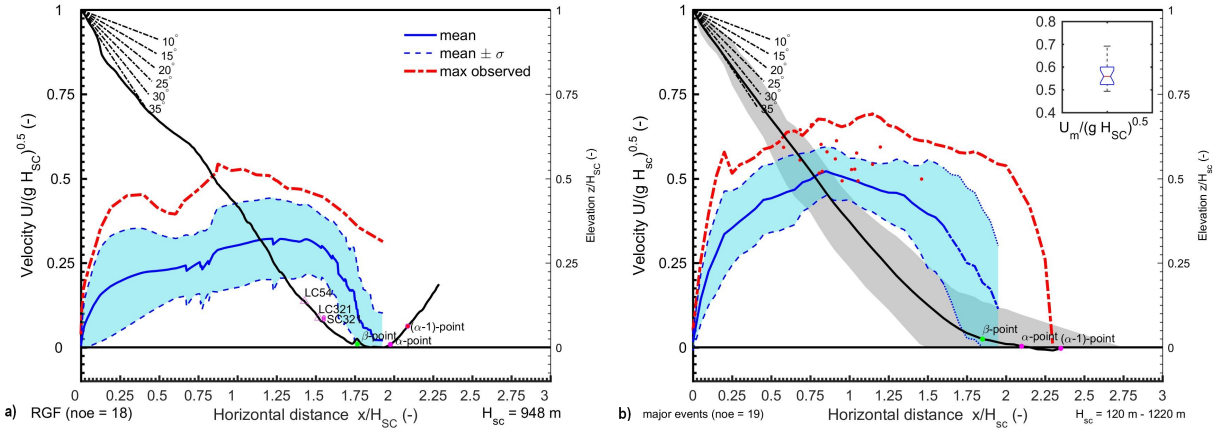

Figure 8: Range of front velocities along the track: a) measurements at the Ryggfonn test site and b) compilation of measurements from various (major) avalanches. The red dots mark the maximum of the different measurements. The black line represents a "mean path" geometry and the gray shaded area the envelope of all geometries. As a reference, the β-point, α and α-1 are shown (for explanation see Lied and Bakkehøi, 1980).

mates are in accordance with, for example, measurements presented by (Sovilla et al., 2006).

3.3 Velocity measurements

Avalanche velocity is an important intensity factor, it is decisive for the dimensioning of mitigation measures, like dams (cf. Jóhannesson et al., 2009) and, first of all, it determines which way the avalanche may take. Therefore, it is also desirable for the practitioner in the field to have an idea about velocities that can be expected in a given path. As all dynamical avalanche models solve the (depth averaged) momentum or velocity equation(s), respectively, velocity measurements along the path and/or at selected locations are also most import for validating those models.

Figure 8 a) presents the measured mean front velocity along the track and the corresponding $\pm\sigma$ range derived from the available measurements at the Ryggfonn test site. Here only those avalanche are considered that reached the main runout area at the valley bottom. This may give an impression of the spectrum of velocities for this specific path. For comparison, figure b) presents a compilation of measurements from "major" dry-mixed avalanches in various paths around the world (cf. Gauer, 2014, 2013, and references therein). Therefore, these velocities may represent the upper range (but not necessary the most extreme) of the expected avalanche velocity along a path. This is in agreement with the measurements from Ryggfonn, from where the highest observed velocities fit well in. The fall height in these cases ranged from about 120 m to 1220 m. To facilitate a comparison, the path geometries are scaled by the fall height H_{SC} and the velocity U by $\sqrt{g\,H_{SC}}$. Then the mean of the observed velocities and their standard deviations are calculated at each point along the track. Similarly, an averaged path profile is calculated, which could be regarded as a kind "standard path". However, one should keep in mind that the mean slope angles of the original profiles cover a typical but limited range. As the inset in figure b) suggests the maximum front velocity (i.e. the heights observed velocity during a single descent) seems to be proportional to the square root of the fall height in the presented cases, that is

$$U_{max} \sim 0.6\sqrt{gH_{SC}} \tag{4}$$

McClung and Schaerer (2006) proposed a similar relation as a kind of upper limit based on observations from Rogers Pass, Canada. Although, some reports indicate that highly fluidized avalanches may have reached higher maximum velocities (Gauer, 2014, and references therein).

3.4 Impact pressure on mast like obstacles

Knowledge about (impact) forces of snow avalanches on narrow obstacles are important for the design of many constructions in avalanche-prone terrain, such as masts of electrical power lines, ski lifts, and cable cars. It is also a prerequisite in the investigation and back calculation of, e.g., forest damage. Recent observations put back in mind that even slow moving avalanches can cause large forces on obstacles (Gauer et al., 2008b; Sovilla et al., 2010; Thibert et al., 2013; Ancey and Bain, 2015). The force on an obstacle might be expressed by

$$F_D \approx \left(C_D + \frac{f_s}{\mathbf{Fr}^2}\right) A\frac{\rho U^2}{2} = C_D^* A\frac{\rho U^2}{2} \tag{5}$$

where **Fr** is the Froude number (= $U/\sqrt{g\,h}$), U the

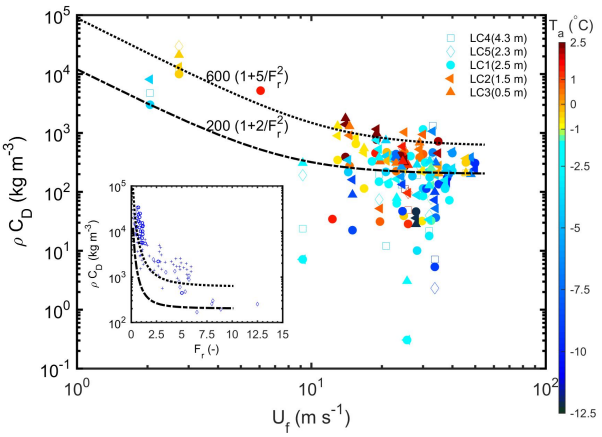

Figure 9: Estimates on ρC_D^* vs. front velocity U_f. Note the log-log-scale. Colors indicate the air temperature. Lines may give a kind of upper envelope for the wet- and dry-snow events. Inset shows similar data adapted from (Sovilla et al., 2008, Fig. 13) as dots.

velocity, h the flow height, A the projected area, and ρ is the avalanche density. The coefficients C_D describes the effect due to the dynamic pressure and f_s the contribution by the static pressure. Both coefficients may depend on the flow properties themselves and on the geometry of the setting. C_D^* represents in this case a lumped drag factor. Figure 9 shows estimates on the combination of flow density and drag factor C_D^* based on observed maximum values of the impact pressure at five different pressure sensors with a size of 1.2×0.6 m^2 and on the front velocity. These values give only a rough estimates as maximum pressures did not necessarily occur at the front and the velocity within in the avalanche may differ from the front velocity. Therefore, the velocity here should only be regarded rather as an indication of the flow state. However, the data give an impression what could be expected. As a reference the plot shows also two example graphs according to (5), using estimates on the typical flow depth. The upper line may give an approximation for wet snow and the lower one for dry snow avalanches. The shown trends are similar to those presented by Sovilla et al. (2008) in their Fig. 13.

3.5 Forces on transmission line cables

In the early years of the Ryggfonn test site a transmission line assembly was mounted in the lower part of the track (Figure 10). The assembly was destroyed by an avalanche in 1990 (see Figure 3). Nonetheless, a limited set of data was obtained during that period. These data are of interest in respect to construction of power lines or cable ways, which could be hit by the powder cloud of an avalanche. They also give some

Figure 10: Transmission line assembly (photo NGI).

indication about the structure of the powder cloud. Figure 11 plots the normalized maximum tension-force vs. height above ground, where F_1 is the tension force at 8 m, F_2 at 12 m and F_3 at 16 m above ground. The graphs show an obvious decrease in the tension force with increasing height about ground, which suggests a similar decrease in the factor ρC_D (cf. equation (5)). An exponential decrease might be a reasonable first guess, that is

$$\frac{F(h)}{F(h_0)} \approx e^{-(e_c \Delta h)}\,; \qquad (6)$$

where h_0 is a reference height and e_c is the rate factor, which depends on the velocity. Generally, the decrease with height is less pronounced with increasing velocity—the forces become more uniform across the flow height. Only two wet snow avalanches in which cases the powder cloud was rather diluted (i.e. F_1 was rather low) fall out of this velocity trend and showed more uniform behavior but low forces.

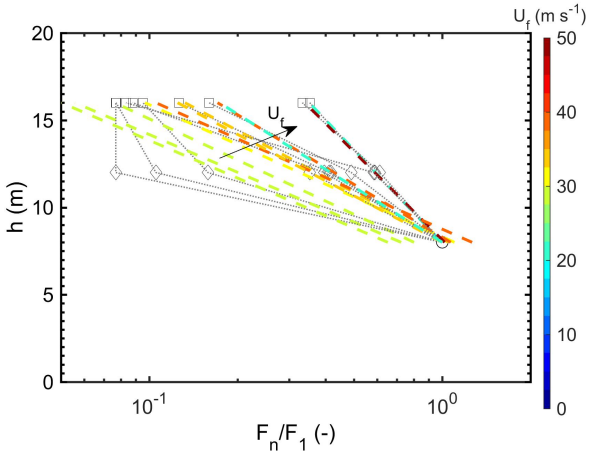

Figure 11: Normalized maximum tension-force vs. height above ground. The dashed lines show exponential fits and the color indicate the front velocity U_f. Note the log-scale.

3.6 Avalanche probability and release height

In avalanche hazard assessment, the probability of an avalanche release in a given path is an important parameter. It is widely accepted that the 3-day new snow depth is an important indictor parameter. However, the conditional probability, $P(A|\mathrm{HNW}_{3d})$ (i.e. the probability of an avalanche for a given HNW_{3d}), may vary from path to path and differs considering a whole region. It probably also varies for different climatological regions. Figure 12 a) shows examples of $P(A|\mathrm{HNW}_{3d})$ for a selection of paths from different regions.

Furthermore, avalanche models require information on the expected fracture depth. A common procedure is to use the 3-day new snow depth for a given retour period and correct for the slope angle (c.f. Salm et al., 1990; Gruber et al., 2002). However, observations, amongst otters from Ryggfonn, suggests using only 3-day new snow sum may underestimate the actual fracture depth. Figure 12 b) shows an approach of using a simple probabilistic model for avalanche release based on Mohr-Coulomb fracture criteria that uses the total snow depth and 3-day new snow depth distribution as input parameter. The inset depicts the corresponding probability distribution of the fracture depth.

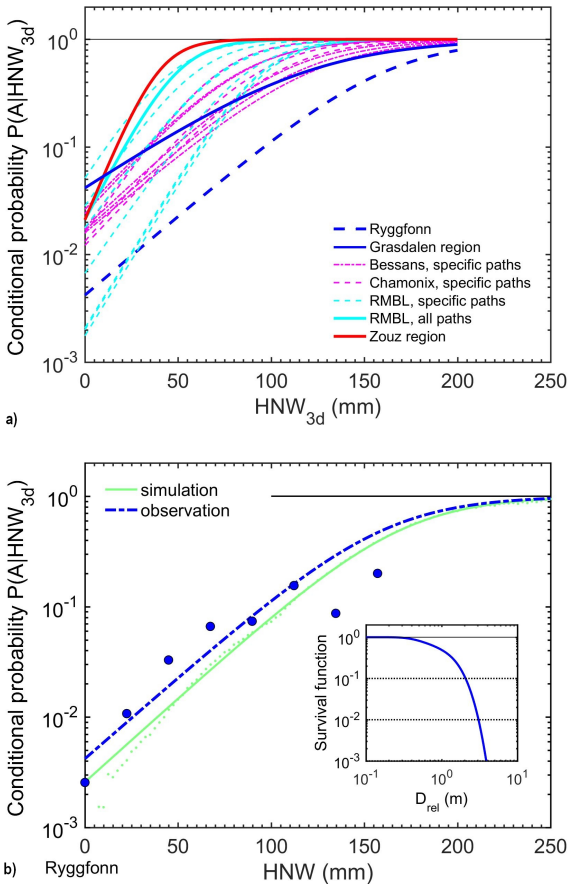

Figure 12: a) Cumulative probability distribution of the conditional probabilities $P(\mathrm{HNW}_{3d}|A)$ for different regions and paths: data adapted from Chamonix and Bessans, France (Meunier et al., 2005); Zouz, Switzerland (Stoffel et al., 1998); Gothic (RBML), Colorado, (courtesy of Billy Barr); Grasdalen region and Ryggfonn path, Norway. b) Comparison between observed and simulated $P(\mathrm{HNW}_{3d}|A)$ for the Ryggfonn path. Lines show the corresponding fits. The inset shows the probability distribution of the expected fracture depth.

4 CONCLUDING REMARKS

Avalanche risk management requires knowledge of runout distances and the corresponding return periods as well as intensity measures. It becomes more and more popular to use numerical models to obtain those required information also in respect to probability distributions, e.g. Eckert et al. (2010). Despite of Perla's rule of thumb "The only rule of thumb in avalanche work is that there is no rule of thumb" (McClung and Schaerer, 2006), it is important to have reference data and/or empirical relations that help to evaluate the performance of those computational runout models, especially in cases where field data are insufficient. A popular empirical relation is certainly the so-called α-β model by Lied and Bakkehøi (1980), which relates the runout angle, α, to the average inclination of the path, β. In this paper now, selected observations from the full-scale avalanche test site Ryggfonn, Norway, are presented and in part compared with observations from other locations to provide further reference data. Some trends can be observed. These trends can provide benchmarks for the evaluation of recently presented approaches of multivariate parameter optimization for avalanche models (Fischer et al., 2015; Eckert et al., 2010).

These empirical data are also helpful for practitioners while delimitating hazard zones.

Although costly and difficult to perform, full-scale avalanche tests are still necessary to obtain in-depth insight in the flow behavior of avalanches and its dependency of the ambient conditions. These experiments provide also reference data for numerical models as well as references for small-scale test to uncover scaling behavior. But also well documented observation from (natural) avalanches in regular paths are desirable to obtain a wider variety of topographic settings.

ACKNOWLEDGMENTS

Parts of this research was carried out through a snow avalanche research grant to NGI from the Ministry of Petroleum and Energy/Norwegian Water Resources and Energy Directorate.

REFERENCES

Ammann, W. J., 1999: A new Swiss test-site for avalanche experiments in the Vallée de la Sionne/Valais. *Cold Regions Science and Technology*, **30**, 2–11, doi:10.1016/S0165-232X(99)00010-5.

Ancey, C. and V. Bain, 2015: Dynamics of glide avalanches and snow gliding. *Reviews of Geophysics*, **53**, 745–784, doi:10.1002/2015RG000491.

Barbolini, M. and D. Issler, 2006: Avalanche Test Sites and Research Equipment in Europe: An Updated Overview. Final-Report Deliverable D8, SATSIE Avalanche Studies and Model Validation in Europe.

Christen, M., J. Kowalski, and P. Bartelt, 2010: RAMMS: Numerical simulation of dense snow avalanches in three-dimensional terrain. *Cold Regions Science and Technology*, **63**, 1–14, doi:10.1016/j.coldregions.2010.04.005.

Eckert, N., M. Naaim, and E. Parent, 2010: Long-term avalanche hazard assessment with a Bayesian depth-averaged propagation model. *Journal of Glaciology*, **56**, 563–586, doi:10.3189/002214310793146331.

Fischer, J. T., A. Kofler, W. Fellin, M. Granig, and K. Kleemayr, 2015: Multivariate parameter optimization for computational snow avalanche simulation. *Journal of Glaciology*, **61**, 875–888, doi:10.3189/2015JoG14J168.

Gauer, P., 2013: Comparison of avalanche front velocity measurements: supplementary energy considerations. *Cold Regions Science and Technology*, **96**, 17–22, doi:10.1016/j.coldregions.2013.09.004.

— 2014: Comparison of avalanche front velocity measurements and implications for avalanche models. *Cold Regions Science and Technology*, **97**, 132–150, doi:10.1016/j.coldregions.2013.09.010.

Gauer, P., H. Breien, D. Issler, K. Kristensen, K. Kronholm, E. Lied, and K. Lied, 2010a: The upgraded full-scale avalanche test-site Ryggfonn, Norway. *Proceedings of the International Snow Science Workshop, Lake Tahoe, CA, October, 17–22, 2010*, 747–752.

Gauer, P. and D. Issler, 2004: Possible erosion mechanisms in snow avalanches. *Annals of Glaciology*, **38**, 384–392, doi:10.3189/172756404781815068.

Gauer, P., D. Issler, K. Lied, K. Kristensen, and F. Sandersen, 2008a: On snow avalanche flow regimes: Inferences from observations and measurements. *Proceedings of the International Snow Science Workshop 2008, September 21- 27, Whistler, British Columbia, Canada*, 717–723.

Gauer, P. and K. Kristensen, 2016: Four decades of observations from NGI's full-scale avalanche test site Ryggfonn —summary of experimental results. *Cold Regions Science and Technology*, **125**, 162–176, doi:10.1016/j.coldregions.2016.02.009.

Gauer, P., K. Kronholm, K. Lied, K. Kristensen, and S. Bakkehøi, 2010b: Can we learn more from the data underlying the statistical $\alpha - \beta$ model with respect to the dynamical behavior of avalanches? *Cold Regions Science and Technology*, **62**, 42–54, doi:10.1016/j.coldregions.2010.02.001.

Gauer, P., K. Lied, and K. Kristensen, 2008b: On avalanche measurements at the Norwegian full-scale test-site Ryggfonn. *Cold Regions Science and Technology*, **51**, 138–155, doi:10.1016/j.coldregions.2007.05.005.

Gruber, U., P. Bartelt, and S. Margreth, 2002: *Kursdokumetation Teil III Anleitung zur Berechnung von Fliesslawinen*. Swiss Federal Institute for Snow and Avalanche Research.

Jóhannesson, T., P. Gauer, D. Issler, and K. Lied, eds., 2009: *The design of avalanche protection dams. Recent practical and theoretical developments*. Number Publication EUR 23339 in Climate Change and Natural Hazards Research Series 2, European Commission, Directorate-General for Research, iSBN 978-92-79-08885-8, ISSN 1018-5593.

Lied, K. and S. Bakkehøi, 1980: Empirical calculations of snow-avalanche run-out distance based on topographic parameters. *Journal of Glaciology*, **26**, 165–177.

Maggioni, M., M. Freppaz, E. Ceaglio, D. Godone, D. Viglietti, E. Zanini, M. Barbero, F. Barpi, M. Borri Brunetto, E. Bovet, B. Chiaia, V. De Biagi, B. Frigo, and O. Pallara, 2012: A new experimental snow avalanche test site at Seehore peak in Aosta Valley (NW Italian-Alps) Part I: preliminary analysis and logistics. *Cold Regions Science and Technology*, **85**, 175–182, doi:10.1016/j.coldregions.2012.09.006.

McClung, D. and P. Schaerer, 2006: *The Avalanche Handbook 3rd edition*. The Mountaineers Books, 1011 SW Klickitat Way, Seattle, Washington 98134.

McClung, D. M. and A. I. Mears, 1991: Extreme value prediction of snow avalanche runout. *Cold Regions Science and Technology*, **19**, 163–175, doi:10.1016/0165-232X(91)90006-3.

Meunier, M., C. Ancey, and D. Richard, 2005: *Conceptual Approach to the Study of Snow Avalanches*. Update sciences & technologies Series.

Naaim, M., F. Naaim-Bouvet, T. Faug, and A. Bouchet, 2004: Dense snow avalanche modeling: flow, erosion, deposition and obstacle effects. *Cold Regions Science and Technology*, **39**, 193–204, doi:10.1016/j.coldregions.2004.07.001.

Salm, B., A. Burkard, and H. U. Gubler, 1990: Berechnung von Fliesslawinen. Eine Anleitung für Praktiker mit Beispielen. Mitt. Eidgenöss. Inst. Schnee- Lawinenforsch. 47, 37 pages, SLF, Davos, Switzerland.

Sampl, P. and M. Granig, 2009: Avalanche simulation with SAMOS-AT. *Proceedings of the International Snow Science Workshop, Davos*, 519–523.

Sovilla, B., P. Burlando, and P. Bartelt, 2006: Field experiments and numerical modeling of mass entrainment in snow avalanches. *Journal of Geophysical Research: Earth Surface*, **111**, F03007(1–16), doi:10.1029/2005JF000391.

Sovilla, B., M. Kern, and M. Schaer, 2010: Slow drag in wet snow avalanche flow. *Journal of Glaciology*, **56**, 587–592, doi:10.3189/002214310793146287.

Sovilla, B., M. Schaer, M. Kern, and P. Bartelt, 2008: Impact pressures and flow regimes in dense snow avalanches observed at the Vallée de la Sionne test site. *Journal of Geophysical Research, Earth-Surfaces*, **113**, F01010(1–14), doi:10.1029/2006JF000688.

Steinkogler, W., B. Sovilla, and M. Lehning, 2014: Influence of snow cover properties on avalanche dynamics. *Cold Regions Science and Technology*, **97**, 121–131, doi:10.1016/j.coldregions.2013.10.002.

Stoffel, A., R. Meister, and J. Schweizer, 1998: Spatial characteristics of avalanche activity in an Alpine valley - a GIS approach. *Annals of Glaciology*, **26**, 329–336.

Thibert, E., H. Bellot, X. Ravanat, F. Ousset, G. Pulfer, M. Naaim, P. Hagenmuller, F. Naaim-Bouvet, T. Faug, K. Nishimura, Y. Ito, D. Baroudi, A. Prokop, P. Schön, A. Soruco, C. Vincent, A. Limam, and R. Héno, 2015: The full-scale avalanche test-site at Lautaret Pass (French Alps). *Cold Regions Science and Technology*, **115**, 30–41, doi:10.1016/j.coldregions.2015.03.005.

Thibert, E., T. Faug, H. Bellot, and D. Baroudi, 2013: Avalanche impact pressure on a plate-like obstacle. *International Snow Science Workshop Grenoble, Chamonix, Mont-Blanc, 2013*, 663670.

UNESCO, 1981: *Avalanche Atlas*. International Commission on Snow and Ice of the International Association of Hydrological Sciences, IAHS.

Wagner, P., 2016: *Kalibrierung des α-β-Modells für das Ermitteln der Auslauflänge von kleinen und mittleren Lawinen*. Master thesis, Institut für Alpine Naturgefahren (IAN), BOKU-Universität für Bodenkultur.